AGU PUBLICATIONS

Geophysical Research Letters

RESEARCH LETTER
10.1002/2014GL059411

Key Points:
- We simulate the M 7.8 ShakeOut earthquake scenario for an elastoplastic medium
- Peak ground velocities are reduced by 30–70% compared to a viscoelastic medium
- These reductions are mostly caused by plastic yielding in the fault zone

Supporting Information:
- Readme
- Figure S1
- Movie S1

Correspondence to:
D. Roten,
droten@sdsc.edu

Citation:
Roten, D., K. B. Olsen, S. M. Day, Y. Cui, and D. Fäh (2014), Expected seismic shaking in Los Angeles reduced by San Andreas fault zone plasticity, *Geophys. Res. Lett.*, *41*, 2769–2777, doi:10.1002/2014GL059411.

Received 5 MAR 2014
Accepted 25 MAR 2014
Accepted article online 12 APR 2014
Published online 23 APR 2014

Expected seismic shaking in Los Angeles reduced by San Andreas fault zone plasticity

D. Roten[1,2], K. B. Olsen[3], S. M. Day[3], Y. Cui[4], and D. Fäh[1]

[1]Swiss Seismological Service, ETH Zurich, Zurich, Switzerland, [2]Now at San Diego Supercomputer Center, La Jolla, California, [3]Department of Geological Sciences, San Diego State University, San Diego, California, USA, [4]San Diego Supercomputer Center, La Jolla, California, USA

Abstract Computer simulations of large ($M \geq 7.8$) earthquakes rupturing the southern San Andreas Fault from SE to NW (e.g., ShakeOut, widely used for earthquake drills) have predicted strong long-period ground motions in the densely populated Los Angeles Basin due to channeling of waves through a series of interconnected sedimentary basins. Recently, the importance of this waveguide amplification effect for seismic shaking in the Los Angeles Basin has also been confirmed from observations of the ambient seismic field. By simulating the ShakeOut earthquake scenario (based on a kinematic source description) for a medium governed by Drucker-Prager plasticity, we show that nonlinear material behavior could reduce the earlier predictions of large long-period ground motions in the Los Angeles Basin by up to 70% as compared to viscoelastic solutions. These reductions are primarily due to yielding near the fault, although yielding may also occur in the shallow low-velocity deposits of the Los Angeles Basin if cohesions are close to zero. Fault zone plasticity remains important even for conservative values of cohesions, suggesting that current simulations assuming a linear response of rocks are overpredicting ground motions during future large earthquakes on the southern San Andreas Fault.

1. Introduction

The southern part of the right-lateral strike-slip San Andreas Fault (SAF) represents a major source of seismic hazard in southern California and northern Mexico [e.g., *Field et al.*, 2009]. Because no major event has ruptured the portion south of Parkfield since the 1857 Fort Tejon earthquake, the southern segments of the SAF have accumulated a slip deficit of 5–6 m and have the potential to produce an earthquake with a magnitude as large as M_w 7.8 [*Weldon et al.*, 2004]. To quantify the ground motions that must be expected from such an event, repeated simulation efforts have been carried out in recent years [e.g., *Olsen et al.*, 1995; *Graves*, 1998; *Olsen et al.*, 2006]. In the framework of the 2008 ShakeOut emergency response and preparedness exercise, numerical simulations of a M_w 7.8 earthquake on the southern SAF were independently performed by three different groups [*Bielak et al.*, 2010] for a maximum frequency of 0.5 Hz. The source model for the ShakeOut scenario was imposed kinematically, with slip distribution and rupture times defined through expert opinion, empirical relationships, and previously published studies [*Graves et al.*, 2008]. All three numerical methods that simulated the ShakeOut earthquake scenario produced very similar results and predicted strong amplification in the Los Angeles Basin (LAB), with peak ground velocities (PGVs) exceeding 1 $m \cdot s^{-1}$ [*Bielak et al.*, 2010; *Graves et al.*, 2008]. Strong amplifications in the LAB for a SE-NW propagating M 7.7 rupture were already predicted by *Olsen et al.* [2006] from the earlier TeraShake simulations and attributed to channeling of seismic waves along a string of sedimentary basins, which form an effective waveguide connecting the SAF with the LAB in the Southern California Earthquake Center (SCEC) Community Velocity Model (CVM-4) [*Magistrale et al.*, 2000]. Subsequent studies revealed that the amount of shaking in the LAB is very sensitive to the kinematically imposed rupture speed [*Graves et al.*, 2008], with stronger shaking generated from faster rupture velocities. Using adjoint simulations, *Day et al.* [2012] showed that the highest excitation in the LAB would occur from super shear (or energetically forbidden subshear, super Rayleigh) rupture speeds in the segment between the Cajon Pass and the northern Coachella valley. Spontaneous rupture models, which simulate the propagation of the rupture based on an initial stress distribution and a fracture criterion, result in much lower PGV extremes in the LAB, with a reduction factor of 2–3 compared to kinematic rupture models [*Olsen et al.*, 2008, 2009].

The signature of a waveguide amplification effect that would lead to strong shaking in the LAB during SE-NW propagating ruptures on the SAF is not only found in synthetic data from computer simulations but has also been identified in observations of the ambient seismic noise. In the recent San Andreas Virtual Earthquake - Los Angeles (SAVELA) experiment [*Denolle et al.*, 2014] empirical Green's functions were extracted from the ambient seismic field and used to predict long-period ground motions for a suite of *M* 7.15 scenario earthquakes on the SAF. LAB shaking levels found by SAVELA confirmed the predictions of the earlier CyberShake simulations [*Graves et al.*, 2011a] that used a similar ensemble of scenario earthquakes, thereby providing observational evidence for the presence of a waveguide west of the San Gorgonio pass.

Numerical models of large earthquakes on the SAF published to date share the assumption of a linear viscoelastic stress-strain relationship in the rocks surrounding the rupture. Methods that predict amplifications from observations of ambient noise [e.g., SAVELA, *Denolle et al.*, 2014] or weak ground motions [e.g., *Field et al.*, 1997; *O'Connell*, 2008] are also inherently assuming linear material behavior. However, it has long been suggested that the high stresses at the rupture front exceed the strength of crustal rock [*Andrews*, 1976], leading to absorption of rupture energy by plastic yielding. Effects of near-fault plasticity on rupture dynamics have received considerable attention in recent years [e.g., *Andrews*, 2005; *Ma and Andrews*, 2010; *Duan and Day*, 2008; *Dunham et al.*, 2011; *Gabriel et al.*, 2013]. It has also been suggested that the large strains induced by energetic long-period surface waves in the LAB may give rise to nonlinear behavior of the shallow sedimentary rock [*Joyner*, 2000; *Sleep*, 2010]. In this paper, we investigate the effect of nonlinear material behavior during large earthquakes on the southern segment of the SAF by simulating the ShakeOut scenario earthquake for materials governed by viscoelastoplasticity.

2. Modeling Wave Propagation in an Elastoplastic Medium

We use the scalable AWP-ODC (Anelastic Wave Propagation, *Olsen et al.* [2006], *Day and Bradley* [2001], *Cui et al.* [2010]) finite difference code to model 0–0.5 Hz wave propagation resulting from the kinematic ShakeOut source description [*Graves et al.*, 2011b; *Bielak et al.*, 2010]. Nonassociated (yielding occurs in shear) Drucker-Prager plasticity, regularized using time-dependent relaxation [*Andrews*, 2005], was implemented in AWP-ODC following the return map algorithm, in accordance with guidelines of the SCEC/USGS (U.S. Geological Survey) dynamic earthquake rupture code verification exercise [*Harris et al.*, 2011]. The Drucker-Prager yield stress,

$$Y(\tau) = \max\left(0, c\cos\varphi - (\tau_m + P_f)\sin\varphi\right), \tag{1}$$

is a function of the cohesion c, the angle of internal friction φ, the fluid pressure P_f, and the mean stress τ_m (negative in compression). The Drucker-Prager yield condition requires that

$$F(\tau) = \sqrt{J_2(\tau)} - Y(\tau) \le 0, \tag{2}$$

where J_2 is the second invariant of the stress deviator, $\mathbf{s}$.

Representative values of fluid pressure P_f were calculated assuming hydrostatic conditions and a groundwater table located at the surface. Although considerable drawdown of the water table has taken place in the Los Angeles Basin over the past century due to ground water pumping, recharge is keeping the piezometric surfaces shallow in several areas, e.g., Whittier Narrows [*Reichard et al.*, 2003]. For the computation of the initial stress tensor, we assumed a NNE-SSW direction of the major principal stress σ_1, representative of the regional stress field in central and southern California [e.g., *Flesch et al.*, 2000; *Townend and Zoback*, 2004]. The intermediate principal stress, σ_2, was taken as vertical and computed from the lithostatic load. We further assumed that the major principal stress is twice as high as the minor principal stress, i.e., $\sigma_1 = 4/3\sigma_2$ and $\sigma_3 = 2/3\sigma_2$. With an average angle of 68° between the major principal stress and the SAF in southern California [*Townend and Zoback*, 2004], this yields a shear to normal stress ratio of ~0.2 on the fault, close to the characteristic lower limit that supports sustained pulse-like rupture [e.g., *Zheng and Rice*, 1998; *Noda et al.*, 2009; *Dunham et al.*, 2011; *Shi and Day*, 2013].

Since the values of the friction angle φ and cohesion c for southern California are poorly constrained, we derive them from known geophysical properties defined in the CVM-4. We used $\varphi = 45°$ in hard rock (shear-wave velocity $v_s \ge 2500$ m·s^{-1}) and $\varphi = 35°$ in alluvium and soft rock (shear-wave velocity $v_s < 2500$ m·s^{-1}). The greatest uncertainty concerns the cohesion c, which may vary over several orders of magnitude, from zero in cohesionless shallow sedimentary rock (such as sands) to hundreds of MPa in crystalline rock. Here we turn to petroleum industry results, where empirical equations have been developed

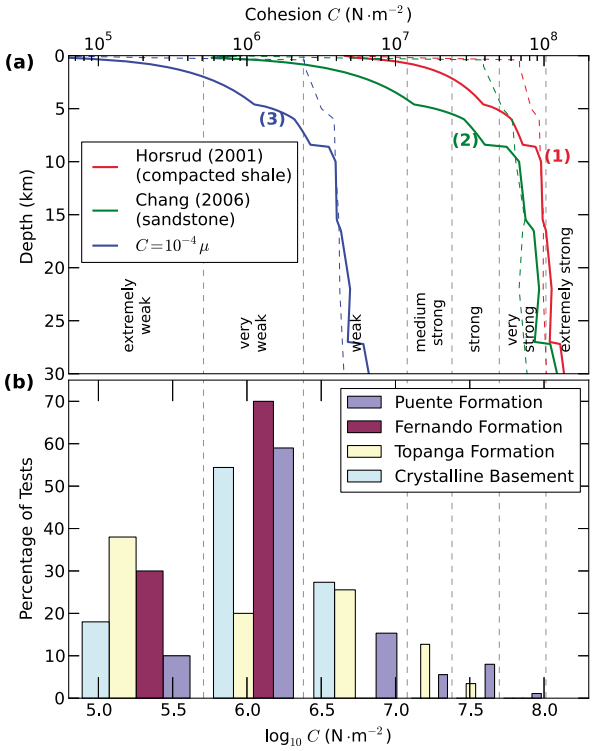

Figure 1. (a) Cohesion as a function of depth at site **dla** in the LAB (solid) and at site **clt** near the SAF (dashed) for the three different equations. (b) Histogram with cohesions determined from laboratory tests in four different formations underlying the LAB [*CH2M Hill*, 2009] (computed from unconfined compressive strengths).

which relate sedimentary rock strength to known physical properties [e.g., *Chang et al.*, 2006]. Such relations use the unconfined compressive strength, q_u, which we relate to cohesion using the conservative estimate of $c = q_u/2$ [e.g., *Jaeger et al.*, 2007]. We tested three different cohesion models 1–3 that to our knowledge cover the realistic range of values in the area. For model 1 the cohesion (MPa) was defined following an empirical relation for compacted shale [*Horsrud*, 2001]:

$$c = 3.61\, E^{0.712}, \tag{3}$$

where E is Young's modulus (GPa). For model 2 we adopted an empirical relation for sandstones [*Chang et al.*, 2006] that defines c (MPa) from the interval velocity Δt (i.e., the inverse of the P wave velocity, in μs/ft):

$$c = 0.7069 \times 10^7 (\Delta t)^{-3}. \tag{4}$$

Figure 1a shows the cohesion as a function of depth for site **dla** (Cerritos) in the LAB and site **clt** (Colton) close to the SAF. For model 1 cohesions range from ~5 MPa at the surface to more than 100 MPa in deep bedrock. Model 2 predicts cohesions of ~0.7 MPa near the surface and values similar to model 1 in bedrock. Laboratory determined cohesions in the Cenozoic sedimentary rocks underlying the LAB [*CH2M Hill*, 2009], however, are below 2.4 MPa for the majority of samples (Figure 1b). Furthermore, many previous studies on rupture dynamics in nonlinear media used cohesions between 0 and 10 MPa [e.g., *Andrews*, 2005; *Ma and Andrews*, 2010; *Dunham et al.*, 2011]. For this reason, we sought to define a third cohesion model, which results in cohesions in the 0 to 10 MPa range while still exhibiting a depth dependency. In model 3 the cohesion is defined from the shear modulus μ (Pa),

$$c = 10^{-4}\, \mu. \tag{5}$$

which yields a cohesion of ~50 kPa near the surface and a maximum cohesion of 6.7 MPa in deep bedrock (Figure 1a). A physical explanation for the low cohesion in model 3 could be the result of fracture generation over numerous earthquake cycles. The simulations were carried out in the CVM-4 [*Magistrale et al.*, 2000] with the minimum shear velocity set to 500 m·s^{-1}, as for the previous ShakeOut simulations (Figure 2a).

3. Reduction of Ground Motions by Plastic Yielding

PGVs obtained for a linear viscoelastic medium (Figure 2b) exceed 1 m·s^{-1} inside a large area along the main waveguide connecting the San Bernardino Basin (SBB) and the LAB, with PGVs above 2 m·s^{-1} in isolated patches (e.g., Whittier Narrows, site **rus**). When plasticity based on cohesion model 2 is taken into account, PGVs remain generally below 1 m·s^{-1} in the LAB, with the exception of a small streak in the Whittier Narrows corridor (Figure 2c). Plasticity also results in a reduced directivity toward the NW and reduced PGVs in the SBB.

Figure 3 compares the reduction in PGVs resulting from the three different cohesion models with respect to the viscoelastic solution. When using relation 1 (Figure 3a), which represents the most conservative cohesion model we tested, PGV reductions of more than 30% are obtained for a large area in the LAB,

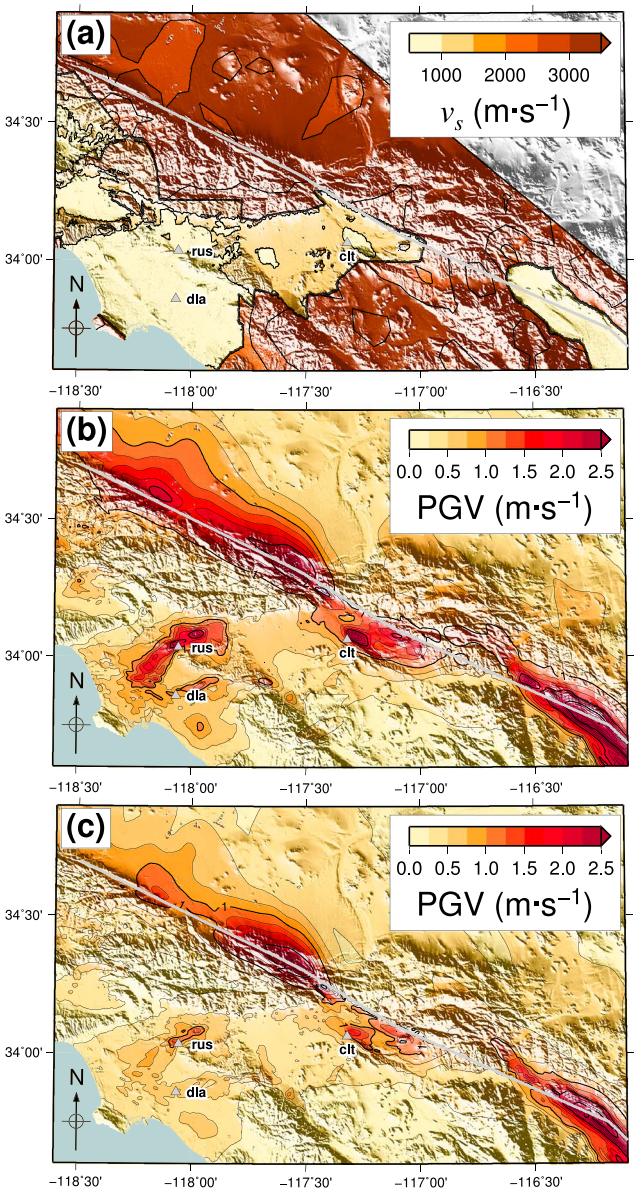

Figure 2. (a) Shear-wave velocity v_s at 200 m depth defined from CVM-4. (b) ShakeOut horizontal peak ground velocities obtained for a viscoelastic medium, and (c) an elastoplastic medium using cohesion model 2.

with reductions above 50% inside smaller patches. PGV reductions of 30–40% are also observed in the San Gabriel mountains north of the LAB, reflecting reduced source directivity. For cohesion model 2 (Figure 3b), PGVs in the LAB are reduced by up to 60%, with reductions above 30% observed inside a larger area compared to cohesion model 1. If cohesions are defined using model 3, plasticity reduces PGVs by more than 60% inside a wide region along the main waveguide, with reductions above 30% virtually everywhere in the LAB and reductions of up to 70% in localized areas (Figure 3c). Note that decreasing the artificially high minimum *S* wave velocity of the ShakeOut simulations (500 m/s) would further amplify these reductions in model 3. Figure 4 shows velocity seismograms obtained by linear viscoelastic and elastoplastic simulations with the three cohesion models at three locations [*Graves et al.*, 2008]: **clt** in the SBB, **rus** in the Whittier Narrows corridor, and **dla** in the LAB.

To identify regions of energy loss due to plastic yielding, we saved the final principal plastic strain η (calculated as the maximum eigenvalue of the final plastic strain tensor) inside the computational volume down to

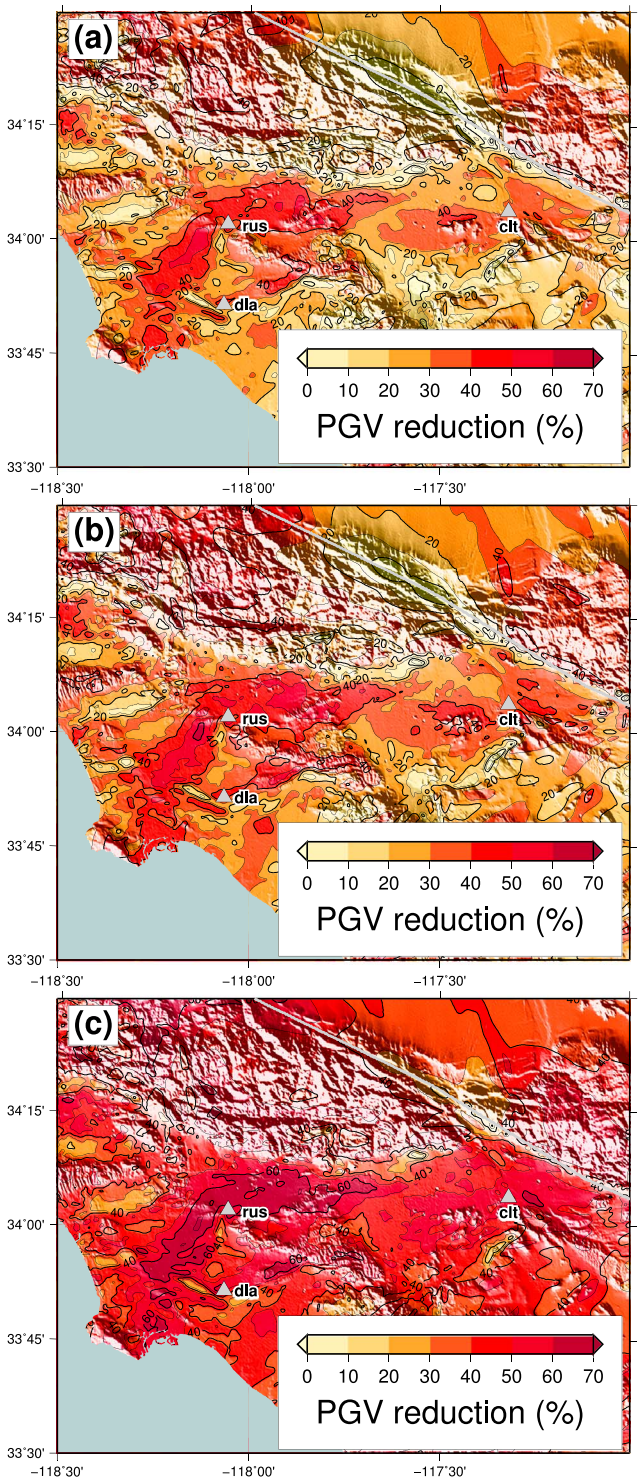

Figure 3. Reduction in horizontal peak ground velocities (%) obtained with cohesion models (a) 1, (b) 2, and (c) 3 with respect to the viscoelastic solution.

16 km depth. Figure 5a shows η at 200 m depth for cohesion model 1. Permanent deformation occurs only inside a confined, less than 1 km wide zone surrounding the fault (enlarged area in Figure 5a). On the other hand, permanent deformation occurs in a wide zone around the fault for cohesion model 3 (Figure 5b), with the level of deformation decreasing with increasing distance from the rupture. For this model we also observe nonlinear behavior in the sedimentary deposits of the LAB/SBB, which results in permanent

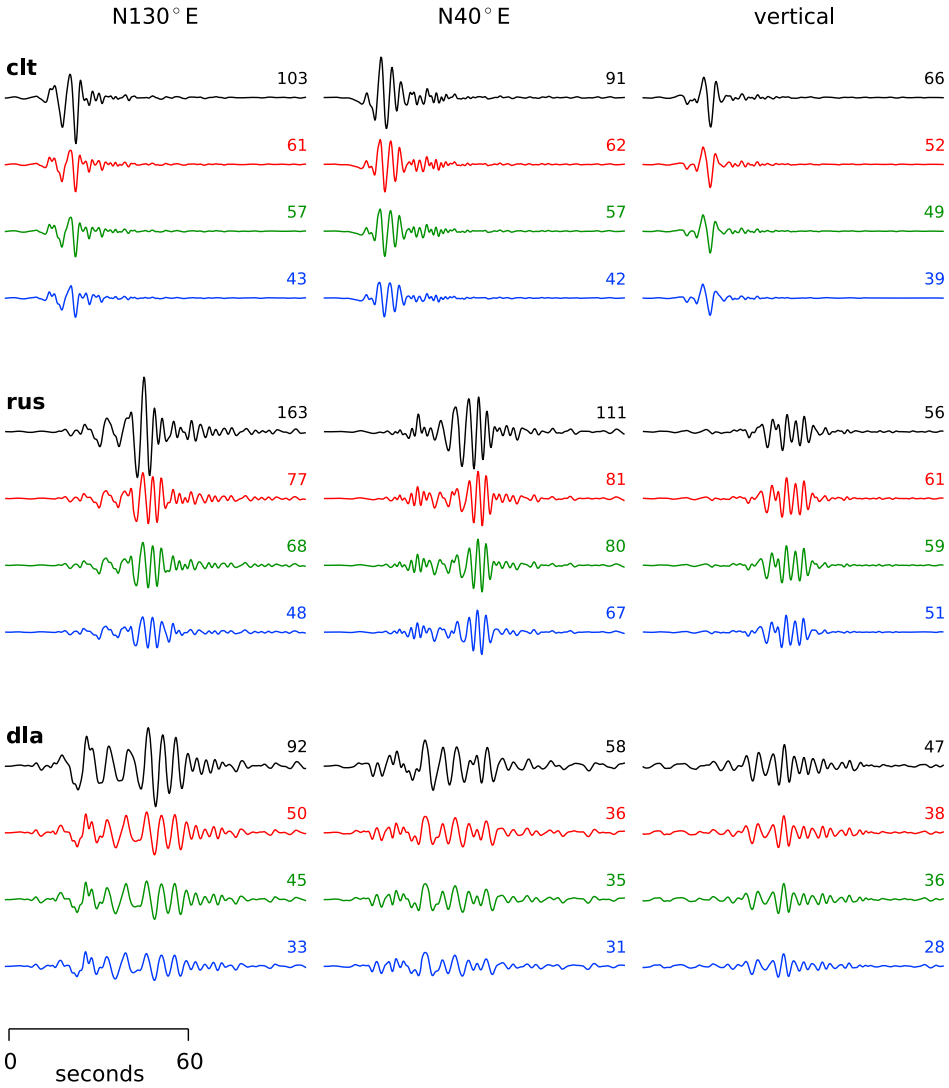

Figure 4. Three-component velocity seismograms obtained for a viscoelastic material (black) and a elastoplastic material using cohesion models 1 (red), 2 (green), and 3 (black). Numbers above each trace denote the peak value in cm·s^{-1}. See Figures 2 and 3 for site locations.

plastic strain especially along the Whittier Narrows corridor. At depths larger than a few km, plastic strain occurs only inside a narrow damage zone around the fault for both cohesion models 1 and 3 (Figures 5c and 5d, respectively). For cohesion model 3 the damage zone widens dramatically near the surface, forming a "flower-like" structure characteristic of real faults [*Ma and Andrews*, 2010].

To analyze the sensitivity of ground motions to the initial stress field in the vicinity of the SAF, we also performed an elastoplastic simulation for cohesion model 2 with the major principal stress rotated counterclockwise by 30° (pointing to N7.5°W). This direction was chosen because stress measurements in deep boreholes show that maximum horizontal stresses near the SAF are rotated to 30–60° with respect to the fault strike [*Scholz*, 2002]. Peak ground velocities in the LAB resulting from this initial stress model (supporting information Figure S1a) are comparable with the values obtained from the original stress model (Figure 5c) and reduced by up to 50% with respect to the viscoelastic model (supporting information Figure S1b). However, PGV reductions above 40% are observed over a larger region with the modified initial stress model (σ_1 pointing to N7.5°W) compared to the original initial stress model (σ_1 pointing to N22.5°E; Figure 3b).

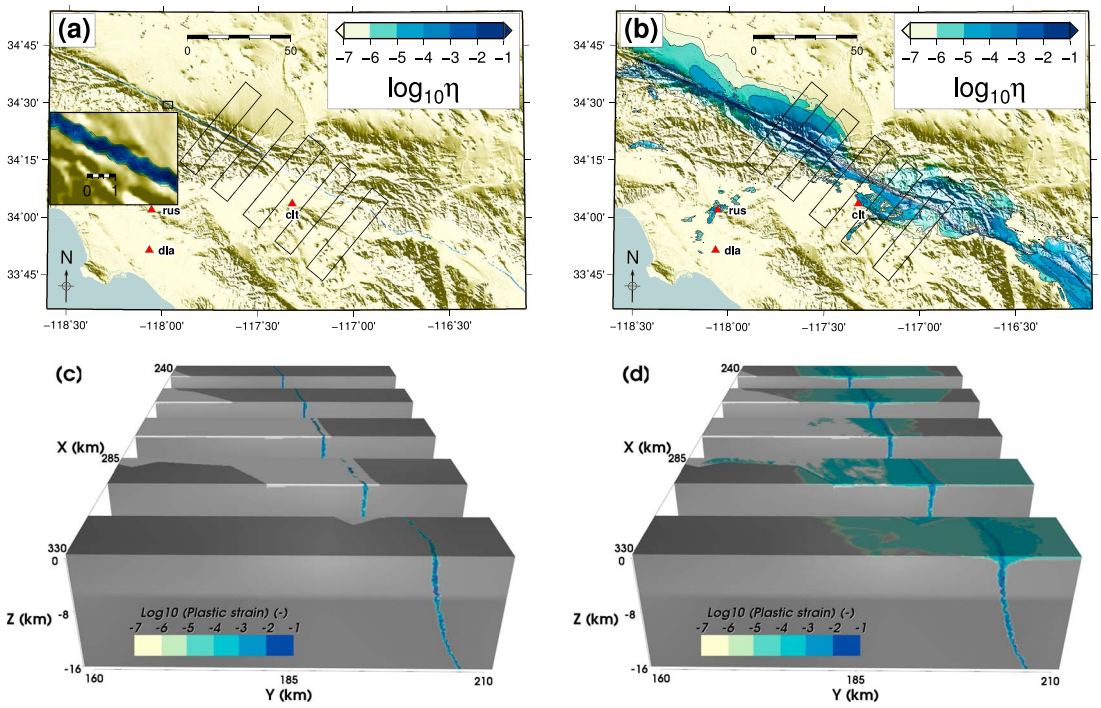

Figure 5. Principal plastic strain η at 200 m depth obtained from cohesion models (a) 1 and (b) 3, with location of cross sections. Plastic strain η (indicated by green-blue shades) on five cross sections through the SAF (view toward NW) for cohesion models (c) 1 and (d) 3. Gray shades reflect shear-wave velocity.

4. Discussion and Conclusions

We have shown that nonlinear effects can significantly reduce the expected long-period ground motions for a large earthquake on the southern SAF. This is somewhat surprising, as nonlinear effects, albeit mostly studied for vertically incident SH waves, are assumed to be effective only at higher frequencies [e.g., *O'Connell*, 2008]. The localization of permanent plastic strain to the fault zone in our simulations shows that the reduction of PGVs can be attributed entirely to plasticity immediately adjacent to the fault for models 1 (Figure 5c) and 2 (not shown). For the frequency range considered in the ShakeOut scenario (0–0.5 Hz), nonlinear behavior in the shallow sedimentary rock of the LAB becomes only important if the sediments are assumed to be nearly cohesionless, as in model 3. Nevertheless, the greatest reductions in PGVs (compared to a viscoelastic solution) are observed on the soft shallow sedimentary rock in the waveguide (Figure 3) for all the three cohesion models. The near-fault elastic peak shear strains greatly exceed laboratory-established thresholds (10^{-5}–10^{-4}) for the onset of strain-amplitude-dependent damping [e.g., *Vucetic*, 1994], with associated large peak shear stresses. We believe that near-fault plasticity limits the peak stresses of strong directivity pulses that would otherwise be channeled into the SBB, thereby leading to a reduction of waveguide amplification and therefore to a disproportionate reduction of PGVs in the LAB.

Our simulations show that the choice of cohesion has a notable impact on the level of ground motions in the LAB, although the effect of cohesion is only pronounced in the inelastic zone near the surface. The three cohesion models used in this study were chosen to cover a broad range of possible rock strengths but are not based on a detailed representation of cohesions in the different sedimentary formations and basement rocks. For example, we neglected the presence of a weakened damage zone surrounding the fault (not resolved sufficiently accurately by the current grid resolution of 200 m), which would typically be characterized by a lower cohesion compared to surrounding intact bedrock [e.g., *Duan and Day*, 2010]. However, our simulation results show that nonlinearity in the fault zone is important even for conservative values of cohesion (as in model 1), suggesting that current simulations based on a linear behavior of rocks are overpredicting the level of ground motion in the LAB during future large earthquakes on the southern SAF. This would have far-reaching implications on earthquake emergency planning scenarios that are based on ground motions predicted with linear wave propagation models, such as the damage scenario of the 2008

Great California ShakeOut [e.g., *Porter et al.*, 2011; *Lynch et al.*, 2011; *Wein et al.*, 2011; *Wein and Rose*, 2011; *Muto and Krishnan*, 2011].

The reduction of peak velocities in our models caused by mostly shallow, near-fault nonlinear effects may have important implications for the scaling of ground motion intensities between surface-rupturing and buried earthquakes. All other conditions equal, our results suggest that earthquakes producing surface rupture may generate smaller peak ground motions due to (predominantly near-fault) nonlinear effects on the produced wave trains, as compared to events on buried faults. *Somerville* [2003] and others observed such trends in ground motion records from historical earthquakes, and our findings provide an alternative or complementary explanation for these observations, as compared to previous mostly rupture dynamics reasoning [e.g., *Dalguer et al.*, 2008]. Ground motion intensities are often presented in terms of ground motion prediction equations, where our results may provide a means to understand and potentially decrease the uncertainty related to the source terms.

More research is warranted into the effect of plasticity on LAB ground motion levels, especially for simulations based on spontaneous rupture models, including cycles of earthquakes on the same fault systems. Future studies would benefit from the extension of community structural models to include information on plastic parameters such as the angle of internal friction φ and cohesion c, in addition to viscoelastic parameters. Community stress models will allow a more precise definition of initial stresses in the medium and contribute to more accurate predictions of ground motions based on physics-based simulations.

Acknowledgments

This research was supported through a contract with the Swiss Nuclear Safety Inspectorate (ENSI), by NSF awards OCI-1148493 (SI2-SSI), EAR-1135455 (FESD), and Southern California Earthquake Center award 13094. SCEC is funded by NSF Cooperative Agreement EAR-1033462 and USGS Cooperative Agreement G12AC20038. Compute resource used for this research is on Kraken at the National Institute for Computational Sciences (http://www.nics.tennessee.edu), the University of Tennessee, and supported by XSEDE under National Science Foundation grant number OCI-1053575. We thank Norman Sleep and an anonymous reviewer for their valuable comments that helped to improve the manuscript.

The Editor thanks Norman Sleep and an anonymous reviewer for their assistance in evaluating this paper.

References

Andrews, D. (1976), Rupture propagation with finite stress in antiplane strain, *J. Geophys. Res.*, *81*(20), 3575–3582.

Andrews, D. (2005), Rupture dynamics with energy loss outside the slip zone, *J. Geophys. Res.*, *110*, B01307, doi:10.1029/2004JB003191.

Bielak, J., et al. (2010), The ShakeOut earthquake scenario: Verification of three simulation sets, *Geophys. J. Int.*, *180*(1), 375–404.

CH2M Hill (2009), SR-710 Tunnel Technical Study, Los Angeles County, California, *Draft geotechnical summary report*, California Department of Transportation.

Chang, C., M. Zoback, and A. Khaksar (2006), Empirical relations between rock strength and physical properties in sedimentary rocks, *J. Pet. Sci. Eng.*, *51*(3), 223–237.

Cui, Y., et al. (2010), Scalable earthquake simulation on petascale supercomputers, *Proceedings of SC10, November 13-19,* New Orleans, La.

Dalguer, L. A., H. Miyake, S. M. Day, and K. Irikura (2008), Surface rupturing and buried dynamic-rupture models calibrated with statistical observations of past earthquakes, *Bull. Seismol. Soc. Am.*, *98*, 1147–1161.

Day, S., and C. Bradley (2001), Memory-efficient simulation of anelastic wave propagation, *Bull. Seismol. Soc. Am.*, *91*(3), 520–531.

Day, S., D. Roten, and K. Olsen (2012), Adjoint analysis of the source and path sensitivities of basin-guided waves, *Geophys. J. Int.*, *189*(2), 1103–1124.

Denolle, M., E. Dunham, G. Prieto, and G. Beroza (2014), Strong ground motion prediction using virtual earthquakes, *Science*, *343*(6169), 399–403, doi:10.1126/science.1245678.

Duan, B., and S. Day (2010), Sensitivity study of physical limits on ground motion at Yucca Mountain, *Bull. Seismol. Soc. Am.*, *100*(6), 2996–3019.

Duan, B., and S. M. Day (2008), Inelastic strain distribution and seismic radiation from rupture of a fault kink, *J. Geophys. Res.*, *113*, B12311, doi:10.1029/2008JB005847.

Dunham, E. M., D. Belanger, L. Cong, and J. E. Kozdon (2011), Earthquake ruptures with strongly rate-weakening friction and off-fault plasticity, Part 1: Planar faults, *Bull. Seismol. Soc. Am.*, *101*(5), 2296–2307.

Field, E. H., P. A. Johnson, I. A. Beresnev, and Y. Zeng (1997), Nonlinear ground-motion amplification by sediments during the 1994 Northridge earthquake, *Nature*, *390*, 599–602.

Field, E. H., et al. (2009), Uniform California earthquake rupture forecast, version 2 (UCERF 2), *Bull. Seismol. Soc. Am.*, *99*(4), 2053–2107.

Flesch, L. M., W. E. Holt, A. J. Haines, and B. Shen-Tu (2000), Dynamics of the Pacific-North American plate boundary in the western United States, *Science*, *287*(5454), 834–836.

Gabriel, A.-A., J.-P. Ampuero, L. A. Dalguer, and P. M. Mai (2013), Source properties of dynamic rupture pulses with off-fault plasticity, *J. Geophys. Res. Solid Earth*, *118*, 4117–4126, doi:10.1002/jgrb.50213.

Graves, R., et al. (2011a), CyberShake: A physics-based seismic hazard model for southern California, *Pure Appl. Geophys.*, *168*(3-4), 367–381.

Graves, R., B. Aagaard, and K. Hudnut (2011b), The ShakeOut earthquake source and ground motion simulations, *Earthquake Spectra*, *27*(2), 273–291.

Graves, R. W. (1998), Three-dimensional finite-difference modeling of the San Andreas fault: Source parameterization and ground-motion levels, *Bull. Seismol. Soc. Am.*, *88*(4), 881–897.

Graves, R. W., B. T. Aagaard, K. W. Hudnut, L. M. Star, J. P. Stewart, and T. H. Jordan (2008), Broadband simulations for M_W 7.8 southern San Andreas earthquakes: Ground motion sensitivity to rupture speed, *Geophys. Res. Lett.*, *35*, L22302, doi:10.1029/2008GL035750.

Harris, R. A., et al. (2011), Verifying a computational method for predicting extreme ground motion, *Seismol. Res. Lett.*, *82*(5), 638–644.

Horsrud, P. (2001), Estimating mechanical properties of shale from empirical correlations, *SPE Drill. Completion*, *16*(2), 68–73.

Jaeger, J., N. Cook, R. Zimmerman, and R. Zimmerman (2007), *Fundamentals of Rock Mechanics*, Wiley-Blackwell, Hoboken, N. J.

Joyner, W. B. (2000), Strong motion from surface waves in deep sedimentary basins, *Bull. Seismol. Soc. Am.*, *90*(6B), S95–112, doi:10.1785/0120000505.

Lynch, K. P., K. L. Rowe, and A. B. Liel (2011), Seismic performance of reinforced concrete frame buildings in Southern California, *Earthquake Spectra*, *27*(2), 399–418.

Ma, S., and D. Andrews (2010), Inelastic off-fault response and three-dimensional dynamics of earthquake rupture on a strike-slip fault, *J. Geophys. Res.*, *115*, B04304, doi:10.1029/2009JB006382.

Magistrale, H., S. Day, R. Clayton, and R. Graves (2000), The SCEC Southern California Reference Three-Dimensional Seismic Velocity Model Version 2, *Bull. Seismol. Soc. Am.*, *90*(6B), S65—S76.
Muto, M., and S. Krishnan (2011), Hope for the best, prepare for the worst: Response of tall steel buildings to the ShakeOut scenario earthquake, *Earthquake Spectra*, *27*(2), 375–398.
Noda, H., E. M. Dunham, and J. R. Rice (2009), Earthquake ruptures with thermal weakening and the operation of major faults at low overall stress levels, *J. Geophys. Res.*, *114*, B07302, doi:10.1029/2008JB006143.
O'Connell, D. R. (2008), Assessing ground shaking, *Science*, *322*(5902), 686–687.
Olsen, K. B., R. J. Archuleta, and J. R. Matarese (1995), Three-dimensional simulation of a magnitude 7.75 earthquake on the San Andreas Fault, *Science*, *270*, 1628–1632.
Olsen, K. B., S. M. Day, J. B. Minster, Y. Cui, A. Chourasia, M. Faerman, R. Moore, P. Maechling, and T. Jordan (2006), TeraShake: Strong shaking in Los Angeles expected from southern San Andreas earthquake, *Seismol. Res. Lett.*, *77*, 281–282.
Olsen, K. B., S. M. Day, Y. A. Minster, Y. Cui, A. J. Chourasia, D. Okaya, and P. Maechling (2008), Terashake2: Spontaneous rupture simulations of M_W 7.7 earthquakes on the southern San Andreas Fault, *Bull. Seismol. Soc. Am.*, *98*(3), 1162–1185.
Olsen, K. B., et al. (2009), ShakeOut-D: Ground motion estimates using an ensemble of large earthquakes on the southern San Andreas fault with spontaneous rupture propagation, *Geophys. Res. Lett.*, *36*, L04303, doi:10.1029/2008GL036832.
Porter, K., et al. (2011), The ShakeOut scenario: A hypothetical M_W7. 8 earthquake on the southern San Andreas fault, *Earthquake Spectra*, *27*(2), 239–261.
Reichard, E. G., et al. (2003), Geohydrology, geochemistry, and ground-water simulation-optimization of the Central and West Coast Basins, Los Angeles County, California, *Water-Resources Investigations Rep. 03-4065*, U.S. Geological Survey, Sacramento, Calif.
Scholz, C. (2002), Evidence for a strong San Andreas fault, *Geology*, *28*(2), 163–166.
Shi, Z., and S. M. Day (2013), Rupture dynamics and ground motion from 3-D rough-fault simulations, *J. Geophys. Res. Solid Earth*, *118*, 1122–1141, doi:10.1002/jgrb.50094.
Sleep, N. H. (2010), Nonlinear behavior of strong surface waves trapped in sedimentary basins, *Bull. Seismol. Soc. Am.*, *100*(2), 826–832.
Somerville, P. G. (2003), Magnitude scaling of the near fault rupture directivity pulse, *Phys. Earth Planet. Inter.*, *137*, 201–212.
Townend, J., and M. Zoback (2004), Regional tectonic stress near the San Andreas fault in central and southern California, *Geophys. Res. Lett.*, *31*, L15S11, doi:10.1029/2003GL018918.
Vucetic, M. (1994), Cyclic threshold shear strains in soils, *J. Geotech. Eng.*, *120*, 2209–2228.
Wein, A., and A. Rose (2011), Economic resilience lessons from the ShakeOut earthquake scenario, *Earthquake Spectra*, *27*(2), 559–573.
Wein, A., L. Johnson, and R. Bernknopf (2011), Recovering from the ShakeOut earthquake, *Earthquake Spectra*, *27*(2), 521–538.
Weldon, R., K. Scharer, T. Fumal, and G. Biasi (2004), Wrightwood and the earthquake cycle: What a long recurrence record tells us about how faults work, *Geol. Seismol. Am. Today*, *14*, 4–10.
Zheng, G., and J. R. Rice (1998), Conditions under which velocity-weakening friction allows a self-healing versus a cracklike mode of rupture, *Bull. Seismol. Soc. Am.*, *88*(6), 1466–1483.